HHS Public Access

Author manuscript

J Biomed Mater Res B Appl Biomater. Author manuscript; available in PMC 2016 February 01.

Published in final edited form as:

J Biomed Mater Res B Appl Biomater. 2016 February ; 104(2): 253–262. doi:10.1002/jbm.b.33378.

Influence of MC3T3-E1 preosteoblast culture on the corrosion of a T6-treated AZ91 alloy

Emily K. Brooks[1], **Menachem E. Tobias**[2], **Shuying Yang**[3], **Lawrence B. Bone**[2], and **Mark T. Ehrensberger**[1,2]

[1]Department of Biomedical Engineering, State University of New York at Buffalo, Buffalo, New York

[2]Department of Orthopaedic Surgery, State University of New York at Buffalo, Buffalo, New York

[3]Department of Oral Biology, State University of New York at Buffalo, Buffalo, New York

Abstract

This study investigated the corrosion of artificially aged T6 heat-treated Mg-9%Al-1%Zn (AZ91) for biomedical applications. Corrosion tests and surface analysis were completed both with and without a monolayer of mouse preosteoblast MC3T3-E1 cells cultured on the sample. Electrochemical impedance spectroscopy (EIS) and inductively coupled plasma mass spectroscopy (ICPMS) were used to explore the corrosion processes after either 3 or 21 days of AZ91 incubation in cell culture medium (CCM). The EIS showed both the inner layer resistance (R_{in}) and outer layer resistance (R_{out}) were lower for samples without cells cultured on the surface at 3 days (R_{in} = 2.64 *e*4 Ω/cm^2, R_{out} = 140 Ω/cm^2) compared to 21 days (R_{in} = 3.60 *e*4 Ω/cm^2, R_{out} = 287 Ω/cm^2) due to precipitation of magnesium and calcium phosphates over time. Samples with preosteoblasts cultured on the surface had a slower initial corrosion (3 day, R_{in} = 1.88 *e*5 Ω/cm^2, R_{out} = 1060 Ω/cm^2) which was observed to increase over time (21 day, R_{in} = 2.99 *e*4 Ω/cm^2, R_{out} = 287 Ω/cm^2). Changes in the corrosion processes were thought to be related to changes in the coverage provided by the cell layer. Our results reveal that the presence of cells and biological processes are able to significantly influence the corrosion rate of AZ91.

Keywords

magnesium alloy; corrosion; cell culture; biodegradation; AZ91

INTRODUCTION

Magnesium (Mg) and its alloys are a class of biodegradable metals which have gained increasing interest as potential orthopedic implant materials.[1–4] Mg has mechanical properties similar to those of cortical bone, lessening concerns of stress shielding.[1] Further, several *in vivo* studies have demonstrated the biocompatibility and osteoinductive capabilities of Mg.[5–9] However, orthopedic use of pure Mg has been limited because of its fast corrosion in the complex physiological environment.[10] A range of Mg alloys have been

Correspondence to: M. Ehrensberger; mte@buffalo.edu.

produced and tested in attempt to slow the corrosion of the material to a rate comparable to that of bone regrowth,[11–15] with interest being directed toward Mg-aluminum-zinc alloys due to their commercial availability.[16–21] Studies have shown acceptable cell adhesion on Mg-9%Al-1%Zn (AZ91) *in vitro*,[22] as well as promising *in vivo* biological responses.[9,23] Further, it has been shown that the mechanical properties of porous AZ91 are similar to that of cancellous bone.[24] However, to enhance clinical translation, it is necessary to understand and ideally predict the corrosion processes that will occur *in vivo* after the implantation of a Mg or Mg alloy device.

As a result of different test conditions, a range of corrosion rates have been reported for Mg materials. Numerous studies have revealed that the choice of test electrolyte, especially the presence or absence of proteins, can have significant effects on corrosion of pure magnesium[25] and its alloys including AZ91.[20] The presence of Cl^- is also known to lower the corrosion resistance of Mg,[26] and high amounts of Cl^- in many test electrolytes may be partially responsible for the increased corrosion rates observed *in vitro* compared to *in vivo*.[27] Nevertheless, it has proven difficult to relate Mg corrosion *in vitro* to *in vivo* corrosion rates and processes.[28,29] Among other complexities, cell/material interactions may influence corrosion *in vivo*, but its role is not currently well defined. Previous reports have shown a decrease in AZ91 corrosion when HeLa cells were cultured on the surface for 2–5 h.[30] This highlights that the presence of cells on the surface of Mg alloys may provide a more realistic *in vitro* model. The present study explores how long-term cellular attachment may influence Mg degradation, while also considering how the corrosion processes influence the adhesion of a cellular layer.

The following research focuses on the use of a T6 heat-treated AZ91E alloy. Heat treatment of AZ91 allows for precipitation of a more passive $Mg_{17}Al_{12}$ β phase which may act as a corrosion barrier depending on its matrix distribution.[31,32] The aims of the present study are to understand the corrosion of T6-AZ91 in a physiologically relevant electrolyte, and further to elucidate how the presence of cells may influence the corrosion of T6-AZ91. Specifically, samples of T6-AZ91 were examined after 3 and 21 days of immersion in osteogenic cell culture media both with and without a monolayer of preosteoblast cells cultured on the T6-AZ91 surface. Electrochemical impedance spectroscopy (EIS) was used to assess the electrochemical properties of the interface, and inductively coupled plasma mass spectroscopy (ICPMS) was used to identify the concentration of ions released into solution. Scanning electron microscopy (SEM) and energy-dispersive X-ray spectroscopy (EDS) were used to investigate the surface/cell morphology and the surface chemistry.

MATERIALS AND METHODS

Sample preparation

The material used in this study was an extruded, T6 heat-treated AZ91E alloy (composition Mg-9.0 wt % Al-0.90 wt % Zn-0.1 wt % Si-0.20 wt % Mn-0.002 wt % Fe-0.0005 wt % Ni, Magnesium Elektron, Manchester, NJ). Samples were machined into discs 3 cm in diameter by 0.75 cm in thickness, and the surface of interest was sequentially wet sanded to a 600 grit finish. The sample was cleansed ultrasonically in deionized water for 10 min and sterilized under ultraviolet (UV) light for 30 min. It was then placed in a custom glass chamber that

allowed for concurrent cell culturing and electrochemical testing in a sterile environment.[33] The exposed surface area of the sample was 3.8 cm^2.

Cell culturing

Mouse preosteoblast MC3T3-E1 cells (ATCC#: CRL-2593) were initially cultured within a humidified 37 °C, 5% CO_2 incubator in T75 flasks utilizing alpha minimum essential medium (AMEM, Gibco) supplemented with 10% fetal bovine serum (FBS, Atlanta Biologicals) and 1% penicillin/streptomycin (Gibco). The AMEM used in this study contained sodium bicarbonate ($NaHCO_3$), which in combination with the 5% CO_2 atmosphere within the incubator, provided buffering to maintain the pH around 7.4.

The experiments were initiated by seeding approximately 100,000 cells within 1 mL of media onto the T6-AZ91 specimens in the glass chambers. The cells were allowed 15 min for initial attachment before an additional 7 mL of media was slowly added to the chamber, resulting in a total volume of 8 mL. An additional 5 h was given to allow the cells to adhere to the sample surface before adding osteogenic reagents to the AMEM+10%FBS. The osteogenic media (OM) was produced by adding 0.01*M* β-glycerophosphate (Sigma Aldrich), $10^{-8}M$ dexamethasone (Sigma Aldrich), and 50 μg/mL ascorbic acid-2-phosphate (Sigma Aldrich) to the original media. The chambers were sealed with a breathable membrane, and this was considered day 0. All chambers were stored in the incubator, and the OM was exchanged every third day. All subsequent experiments were performed with T6-AZ91 samples seeded with MC3T3-E1 cells (MC3T3/AZ91) or T6-AZ91 samples immersed in OM without cells (OM/AZ91).

Electrochemical impedance spectroscopy

The EIS was performed after 3 and 21 days of incubation. At these time points, the initial glass chamber was modified to create a three-electrode corrosion cell as shown in Figure 1. Specifically, the T6-AZ91 sample mounted in the bottom of the glass chamber served as the working electrode. The breathable membrane on the glass chamber was replaced with a rubber stopper that suspended a graphite counter electrode and an agar KCl salt bridge. The agar salt bridge electrically connected the silver/silver-chloride (Ag/AgCl) reference electrode in a reference well filled with phosphate buffered saline (PBS, Mediatech) to the working electrode. Connections were made to a potentiostat (Ref 600, Gamry), the electrochemical cell was returned to the incubator, and the open circuit potential (OCP) was monitored for 15 min. Subsequently, EIS was performed about the OCP by applying a 10 mV sinusoidal oscillation over a frequency range of 100 kHz to 5 MHz. After observing a two time constant pattern in the Bode plots, the data was fit to a two-layer circuit model using a complex-non-linear-least-squares method (EIS 300 software, Gamry Instruments). The circuit model consisted of a solution resistor (R_s) in series with two parallel combinations of constant phase elements and resistors ((CPE_{out}, R_{out}), (CPE_{in}, R_{in})). Polarization resistance (R_p) was calculated by summing R_{in} and R_{out} ($R_p = R_{in} + R_{out}$). EIS was performed on three independent samples of OM/AZ91 and MC3T3/AZ91 after 3 and 21 days of incubation.

ICPMS

Concentrations of Mg, Al, and Zn released from the T6-AZ91 samples into the OM were identified using ICPMS. After EIS completion, 2 mL aliquots of the OM were removed from each sample chamber and underwent an acid digestion using optima grade nitric acid (HNO_3, Fisher Scientific) and optima grade hydrogen peroxide (H_2O_2, Fisher Scientific). The 2 mL solution aliquot, 2 mL HNO_3, and 2 mL distilled H_2O were placed in digestion vessels and heated at 100 °C for 20 min. After cooling, an additional 2 mL of HNO_3 were added to each sample. Samples were again heated at 100 °C for 30 min and allowed to cool before adding 1 mL of 30% H_2O_2 dropwise to the solution. The samples were returned to the hot block and heated until evaporation, leaving behind the residual trace metals. In order to determine the concentration of Mg, Al, and Zn ions present in the base media, an additional acid digestion was performed on three samples of OM which had not been incubated with T6-AZ91. ICPMS analysis was performed with a Perkin Elmer Sciex model ELAN DRC-II (Trace Evidence Analysis Facility, Florida International University) after optima grade HNO_3 had been used to prepare the calibration curves. Three independent samples of solution were analyzed for both OM/AZ91 and MC3T3/AZ91 after 3 and 21 days of incubation.

Surface analysis

After 3 and 21 days of immersion, the OM/AZ91 and MC3T3/AZ91 samples were removed from the chamber and rinsed with PBS. The OM/AZ91 samples were allowed to air dry, while MC3T3/AZ91 samples were fixed with 2.5% glutaraldehyde (Fisher Scientific), dehydrated using graded ethanol mixtures up to 100% ethanol, and treated with hexamethyldisilazane (HMDS, Sigma Aldrich). All samples were sputter coated with carbon and subsequently imaged in both secondary electron (SE) and backscattered electron (BSE) modes with a scanning electron microscope (Hitachi SU70). Elemental analysis and characterization of the corrosion layer on 3 and 21 day OM/AZ91 samples was completed using EDS.

Statistical analysis

Comparisons were made between 3 and 21 day samples within groups, as well as between OM/AZ91 and MC3T3/AZ91 groups at 3 and 21 days. A one-way ANOVA with Tukey's *post hoc* tests where appropriate was used to identify statistical differences in EIS parameters. Log transformed data of R_s, R_{out}, R_{in}, C_{out}, and C_{in} was used for statistical analysis due to a wide range in values across the groups. Due to a significant Levene's test, all ion concentrations from ICPMS results and the OCPs of different samples were compared using a Welches ANOVA followed by a Games-Howell *post hoc*. A p values of less than 0.05 was considered significant for all statistical tests. Statistical software (SPSS) was used to perform all statistical calculations.

RESULTS

EIS

The *OCP* values measured preceding EIS testing are presented in Table I. An electropositive shift was observed in the OCP from 3 to 21 days for OM/AZ91. At 21 days, OM/AZ91 samples displayed a more electropositive OCP than MC3T3/AZ91 samples. There was no significant difference in the OCP measured for OM/AZ91 and MC3T3/AZ91 samples at 3 days.

Bode plots resulting from EIS testing of OM/AZ91 and MC3T3/AZ91 samples at 3 and 21 days are presented in Figure 2(a–d). The impedance modulus versus frequency curves are displayed in Figure 2(a,c), while the phase angle versus frequency curves are displayed in Figure 2(b,d). An examination of the figures show plateaus in both the low and mid frequency ranges of the impedance modulus plot and two distinct minima in the phase angle plot. Therefore, all data was fit to a two-layer circuit model corresponding to a two layer corrosion film formed on AZ91. The fitted values of the circuit parameters representing the Faradaic processes at the interface are shown in Figure 3(a,b), while those characterizing the non-Faradaic processes are shown in Figure 4(a–d).

There is a statistical increase in both the outer layer resistance (R_{out}) and the inner layer resistance (R_{in}) for OM/AZ91 samples between 3 and 21 days [Figure 3(a,b)]. Conversely, both R_{out} and R_{in} significantly decrease for MC3T3/AZ91 samples between 3 and 21 days of incubation [Figure 3(a,b)]. The resistance of both layers is statistically higher for MC3T3/AZ91 samples at 3 days (R_{out} = 1060 Ω/cm^2, R_{in} = 1.88 *e*5 Ω/cm^2) than OM/AZ91 samples at 3 days (R_{out} = 140 Ω/cm^2, R_{in} = 2.64 *e*4 Ω/cm^2). The CPE magnitude of the inner (Q_{in}) and outer layer (Q_{out}) remain constant between 3 and 21 days for OM/AZ91 samples [Figure 4(a,b)], while for MC3T3/AZ91 samples both Q_{in} and Q_{out} show a statistical increase from 3 to 21 days [Figure 4(a,b)]. At the 3 day time point, Q_{in} and Q_{out} are larger for OM/AZ91 samples when compared to MC3T3/AZ91 samples [Figure 4(a,b)]. Whereas at the 21 day time point, Q_{in} is higher for MC3T3/AZ91 samples than OM/AZ91 samples [Figure 4(b)]. The CPE exponent of the outer layer (α_{out}) statistically decreases from 3 to 21 days for both OM/AZ91 and MC3T3/AZ91 samples [Figure 4(c)]. Further, MC3T3/AZ91 samples have a higher α_{out} value when compared to OM/AZ91 samples at 3 days [Figure 4(c)].

ICPMS

The concentrations of Mg and Zn ions released into solution as measured by ICPMS are presented in Figure 5(a,b). None of the conditions showed a significant change in the Al concentration released to electrolyte when compared to the base media (Al ions = 51 ± 11 ppm) and therefore the data is not presented. The reported ICPMS results do not correspond to the total accumulation of ions in solution throughout the entire experiment, but rather the amount of ions released during the initial 3 day period (0–3 days) and final 3 day period (18–21 days). Media collected from OM/AZ91 samples at both 3 and 21 days contained higher concentrations of Mg ions than were present in the base media [Figure 5(a)]. The media from 0 to 3 days of OM/AZ91 incubation contained a higher concentration of Mg ions than the media from 18 to 21 days of OM/AZ91 incubation [Figure 5(a)]. A statistically

higher concentration of Mg ions was released to solution for MC3T3/AZ91 samples between 18 and 21 days when compared to the base media [Figure 5(a)]. It is notable that media collected after the initial 0–3 day incubation of MC3T3/AZ91 samples represented the only condition without a significant increase in Mg ion concentration compared to the base media [Figure 5(a)]. MC3T3/AZ91 samples from the final 3 day period showed higher Zn release (~280 ppb) into electrolyte compared to the OM/AZ91 samples and baseline media controls (~30 ppb) [Figure 5(b)].

SEM and EDS

Representative scanning electron micrographs of OM/AZ91 samples before immersion, after 3 days of immersion, and after 21 days of immersion are shown in Figure 6(a–c). Figure 6(a) displays the sample before immersion in OM, the parallel lines result from the polishing procedure. After three days of immersion, two distinct regions were observed on the sample surface: a light region and a darker cracked region [Figure 6(b)]. By 21 days of immersion, the entire surface appeared darker and cracked [Figure 6(c)]. Results from EDS in Table II reveal higher atomic percentages of O, Al, P, and Ca present in the darker region at both 3 and 21 days than the lighter regions found on sections of the 3 day samples.

Micrographs obtained after 3 and 21 days of incubation of MC3T3/AZ91 samples allowed for assessment of the sample surface as corrosion occurred and characterization of cell morphology at the time of fixation [Figure 7(a–d)]. Day 3 low magnification images show an indistinguishable monolayer of well spread cells covering the sample surface [Figure 7(a)]. Higher magnification images at day 3 [Figure 7(c)] show more details including multiple points of cell attachment as well as small gaps between adjacent cells where the AZ91 surface is exposed. At 21 days, the cells have remained well spread and attached to the corroding AZ91 surface [Figure 7(b,d)]. Occasional disruptions to the cell monolayer were also observed at day 21. These specific regions appeared as elliptical openings in the cell layer, and exposed the underlying AZ91 [Figure 7(b,d)]. At day 21, nodular features were also frequently observed within the extracellular matrix, perhaps indicating mineralization of the matrix.

DISCUSSION

The present study focused on corrosion and biocompatibility of a T6-treated AZ91 alloy. Heat treatment produces changes in the microstructure of AZ91, leading to β phase precipitation along the grain boundaries. The size and distribution of the resulting β phase is able to influence the corrosion processes of the alloy.[32,34] For example, heterogeneous distribution of the passive β phase can lead to microgalvanic coupling between the β phase and more active α matrix, accelerating corrosion.[35] A decreased Al content remaining in the α matrix after precipitation of the β phase may also contribute to higher corrosion rates in heat-treated alloys.[36] However, when evenly distributed, the β phase can slow corrosion processes. After 1 h of exposure to 5% NaCl, the rate of the anodic reaction for T6-Mg9Al decreased related to a protective layer forming over the surface when compared to both T4-Mg9Al and pure Mg.[31]

Recently, several authors have tested the corrosion of heat-treated Mg alloys in solutions simulating the physiological environment for biomedical applications.[37–39] It was concluded that a more even aluminum distribution in heat-treated AZ63 samples allowed for the formation of a more protective oxide layer. This resulted in significantly lower corrosion rates than for the untreated samples in simulated body fluid (SBF).[37] Further it has been determined that T6 heat treatment led to a reduction in the corrosion rate of AZ91 in SBF over 168 h of immersion compared to the as received samples.[38] It is important to note that the SBF solutions used in these previous studies were not supplemented with serum containing proteins, which is considered an influential factor in predicting bio-corrosion rates.[25] Another heat-treated alloy, Mg-7.5%Al-0.8%Zn-0.2%Mn, was investigated in Dulbecco's modified eagle medium with 10% fetal calf serum over a 30-h time period.[39] The polarization resistance of the aged samples measured by EIS reached larger values (~800 kΩ/cm^2) than the as received samples (~200 kΩ/cm^2). This was considered to be a combined result of β phase distribution and formation of a protective corrosion product. When EIS was performed on thermally treated AZ91 alloys exposed to complete cell culture medium containing 10% fetal bovine serum for 1 h, a resistance of over 70 kΩ/cm^2 was recorded. This was again attributed to an almost continuous β phase produced after the heat treatment acting as a barrier to corrosion.[40]

Although direct comparisons to an as cast AZ91 alloy were beyond the scope of this work, as expected, our results show higher corrosion resistance of T6-treated OM/AZ91 when compared to as cast AZ91 in the literature. While linear polarization has been used to determine a polarization resistance (R_p) of ~8000 Ω/cm^2 for AZ91 after 3 days of immersion in media with proteins, our calculated R_p ($R_p = R_{in} + R_{out}$) for OM/AZ91 at 3 days exceeded 26,000 Ω/cm^2.[20]

An equivalent circuit model previously used to fit EIS spectra of thermally treated Mg alloys in complete cell culture medium was utilized for data analysis.[39,40] This two layer model can be correlated to the two-layer corrosion film produced on AZ91 consisting of an inner globular layer and outer amorphous porous layer.[41] Over time, it has been reported the inner layer becomes enriched in aluminum, and the presence of Al_2O_3 contributes to the enhanced passivating properties of the inner barrier layer.[41,42] Therefore, for OM/AZ91 samples at 3 and 21 days R_{out} and Q_{out} represent the resistance and non-Faradaic properties of the porous $Mg(OH)_2$ outer layer. While R_{in} and Q_{in} represent the resistance and non-Faradaic properties of the aluminum enriched inner barrier layer.

An increase in both R_{out} and R_{in} of OM/AZ91 over the incubation period indicates that corrosion had slowed over time [Figure 3(a,b)]. It has been proposed that the corrosion of Mg slows over time in complete cell culture medium due to the formation of magnesium and calcium phosphates on the surface acting as a barrier to the corrosion reactions.[21,43] Our SEM and EDS results indicate that similar product formation takes place on T6-treated AZ91 in OM. After three days of immersion, a patchwork of corrosion product is evident on the surface [Figure 6(b)]. The darker appearing region contains higher amounts of O, P, and Ca, as well as lower amounts of Mg when compared to the remainder of the surface (Table II). These changes in surface composition suggest the formation of magnesium and calcium phosphates. By day 21, the entire surface is covered with corrosion product [Figure 6(c)],

and higher atomic percentages of O (70%), P (8.4%), and Ca (4.3%) are present (Table II). The corrosion product formation may contribute to the decrease in α_{out} between 3 and 21 days for OM/AZ91 samples [Figure 4(c)] as it has been reported that the outer layer formed on Mg is often amorphous and nonuniform.[41,43] These changes, along with a decrease in the concentration of Mg ions released to solution (Figure 5), are consistent with a decrease in the corrosion rate for T6-treated AZ91 in biologically relevant media over extended time periods.

An examination of the results for MC3T3/AZ91 samples revealed different trends in corrosion processes over time. Authors have investigated changes in the electrochemical properties of passive biomaterials such as 316 L stainless steel[44] and titanium (Ti)[45,46] when a layer of cells is present on the surface. Using impedance and polarization tests, it was concluded that the presence of cells ultimately caused a decrease in the corrosion resistance of 316 L stainless steel after 7 days of culture, in part due to an accumulation of Cl^- ions at the surface.[44] While others have determined that the impedance of both Ti and titanium-6%aluminum-4%vanadium (Ti64) increased due to the presence of cells and their extracellular matrix after both 4 and 7 days of culture.[46]

In regards to Mg, it is not clearly understood how the presence of cells at the interface of a more active metal may be influencing the electrochemical properties. EIS has been used to explore changes in the corrosion resistance of AZ91 samples with and without HeLa cells cultured on the surface.[30] Although testing was only completed at initial 2 h and 5 h time points, it was determined that the cell layer led to an increase in the charge transfer resistance and the overall impedance. Similarly, others have measured a smaller change in electrolyte pH when Mg samples were incubated with cells and serum compared to samples incubated with Dulbecco's medium alone.[47] While the presence and absence of serum likely impacts the corrosion processes, the pH differences may also, in part, be due to the presence of cells.

We sought to further characterize the electrochemical properties of T6-AZ91 after culturing MC3T3-E1 preosteoblasts on the surface for either 3 or 21 days. For MC3T3/AZ91 EIS results, the physical interpretation of our circuit model was again correlated to the two layer corrosion film composed of an outer $Mg(OH)_2$ porous layer and more compact inner layer with Al_2O_3 present.[41] Effects from the MC3T3 cells were taken to be combined with the characteristics of the film's outer layer (R_{out} and Q_{out}). After 3 days of incubation, MC3T3/AZ91 samples have a statistically higher R_{out} [Figure 3(a)] and R_{in} [Figure 3(b)] and statistically lower Q_{out} [Figure 4(a)] and Q_{in} [Figure 4(b)] when compared to OM/AZ91 samples. These differences are consistent with a more protective, thicker, and passivating layer on the MC3T3/AZ91 samples. In addition, ICPMS results showed no significant increase in Mg ion concentration at 3 days when compared to the base media (Figure 5), suggesting a slower anodic half-cell reaction. Previous work has found that osteoblast-like cell culture on Ti increased the incorporation of phosphorus and calcium in the oxide layer.[48] The increased R_{in} and R_{out} of MC3T3/AZ91 samples at 3 days may in part be due to a similar mechanism of enhanced ion and protein incorporation. In addition, the increased R_{out} may result from the presence of cells acting as a physical barrier to corrosion.

Micrographs of MC3T3/AZ91 samples after 3 days of incubation show well spread and attached cells [Figure 7(a,c)]. A monolayer of cells appears to be spread continuously and evenly over nearly the entire surface of the sample. An increased magnification image after 3 days of culture displays multiple attachments both between cells and from cells to the T6-AZ91 substrate [Figure 7(c)]. The morphological features of these flattened and well attached cells suggest good adhesion of MC3T3-E1 cells after 3 days of culture on corroding T6-AZ91.

Several changes were apparent over the incubation time for MC3T3/AZ91 samples. Between 3 and 21 days, R_{out} and R_{in} decrease [Figure 3(a,b)], while Q_{out} and Q_{in} increase [Figure 4(a,b)]. These changes suggest MC3T3/AZ91 samples become more susceptible to corrosion over time. An examination of the ICPMS results show that at 21 days, there is an increase in the Mg ion concentration compared to the base media (Figure 5), confirming increased degradation.

The decrease in corrosion resistance over time may be related to changes in the coverage provided by the cell layer. After 21 days of incubation, it became apparent that the cellular layer had been disrupted in several areas which appeared as elliptical regions where the AZ91 surface was exposed [Figure 7(b)]. This surface heterogeneity is also suggested by the decrease in α_{out} for MC3T3/AZ91 samples from 3 to 21 days. We propose that the areas of exposed surface result from pockets of hydrogen gas forming under the cell layer over time as corrosion takes place. A result of the overall reaction for Mg corrosion occurring (Eq. 1) is the production of H_2.

$$Mg + 2H_2O \rightarrow Mg^{2+} + 2OH^- + H_2 \quad (1)$$

Just as there is potential for H_2 bubbles to form subcutaneously *in vivo* after Mg implantation,[1] it is possible H_2 bubbles formed beneath the cell layer *in vitro* and eventually caused seams to open in the cell monolayer, leaving areas of the surface exposed. Once these openings in the outer layer had formed, corrosion could occur more freely at these sites, resulting in the observed shifts in EIS spectra and increase in ion release as measured by ICPMS.

Regardless of the openings in the cell layer, the majority of cells remained adhered to the surface at day 21. Cells had grown to confluence over the majority of the surface, indicating that the cells were able to remain attached to and grow on the surface over the 21-day test period even as corrosion of the underlying material was occurring. Throughout the sample, the formation of extracellular matrix was also apparent.

A comparison between OM/AZ91 samples and MC3T3/AZ91 samples at the 21-day time point reveal that despite initial differences in the corrosion resistance, by later time points the corrosion of the two conditions is more comparable. The lack of differences between R_{out}, R_{in}, and Mg ion release indicate that at 21 days, the corrosion resistance and rate of dissolution of MC3T3/AZ91 and OM/AZ91 samples have become similar. Although the difference is minimal, MC3T3/AZ91 Q_{in} is significantly larger than OM/AZ91 Q_{in} at the 21-day time point. It is possible that the slight difference can be attributed to H_2 bubbles

also disrupting any proteins adsorbed on the inner Al_2O_3 layer. Interestingly, Zn ion release, as measured by ICPMS, was significantly increased for MC3T3/AZ91 samples when compared to OM/AZ91 samples at 21 days. However, the mechanism for this increased Zn release from MC3T3 samples is currently unclear.

Limitations of the present study include testing at only an initial and final time point, which allowed for observation of changes, but prevented accurate understanding of when those changes in the cell layer and corrosion resistance may have occurred. Total corrosion and degradation over the 21-day period was not measured, also making it difficult to determine the extent of the impact a layer of cells may have on reducing the corrosion of T6-AZ91.

We have demonstrated that preosteoblasts cultured on T6-AZ91 form a near complete monolayer on the surface at 3 days and that the corrosion resistance is increased as compared to the OM/AZ91 samples. At 21 days the cell monolayer remained robust, but there were occasional openings that reduced the coverage quality with large areas of the AZ91 surface exposed. It was further shown that the corrosion resistance of the MC3T3/AZ91 samples decreased at 21 days was compared to 3 days. Based upon these findings it is proposed that at early time points the near continuous monolayer is acting as a physical barrier to corrosion processes. However, the small intercellular gaps [Figure 7(c)] allows for electrolyte penetration to the AZ91 surface to initiate corrosion, albeit at a reduced rate on a smaller percentage of the surface. This initial corrosion process may involve crevice-type corrosion underneath the cell monolayer that gradually leads to the accumulation of hydrogen gas under the monolayer. Eventually, tension may develop in the cell monolayer as a result of the hydrogen gas accumulation, and force a seam to open in the monolayer to allow the gas to be released. We propose the elliptical openings observed at 21 days were formed in this way and that after this pocket has been created, the underlying substrate in the area is now exposed to the bulk electrolyte for accelerated corrosion. It is also possible that the corrosion processes may now proceed through a galvanic-like mechanism, where areas covered by cells and areas exposed to the bulk electrolyte are coupled together. This results in both OM/AZ91 and MC3T3/AZ91 samples showing similar corrosion resistances after 21 days of immersion or culture. Corrosion and cellular processes on Mg and its alloys could be considered part of a feedback loop, where the corrosion resistance is dependent on the cell layer and biological activity, just as the cell adhesion and monolayer coverage is dependent on the rate of corrosion.

It has been stated that the presence of cells can be a significant aspect of the corrosion processes of metallic materials.[49] Since cells will be present on the implant surface *in vivo*, materials tested *in vitro* should be placed under parallel conditions when possible. Corrosion testing with cells seeded on the material surface may provide more realistic conditions for predicting *in vivo* corrosion of Mg, and contribute to finding a reliable correlation between *in vitro* and *in vivo* corrosion rates.

We have shown that corrosion resistance of T6-AZ91 in complete cell culture medium increases during a 21-day immersion period likely due to formation of corrosion products, including magnesium and calcium phosphates. We further demonstrated that mouse preosteoblast MC3T3-E1 cells cultured on the T6-AZ91 surface limited corrosion of the

material at early time points. The increased corrosion resistance and decreased Mg dissolution after 3 days of culture indicate that the presence of cells on Mg may be acting as a barrier to corrosion reactions. Over time changes in the coverage provided by the cell layer reduced its protective qualities, and the corrosion resistance decreased to values similar to those of control samples.

Acknowledgments

Contract grant sponsor: Basic Research Grant from the Orthopedic Trauma Association

REFERENCES

1. Staiger MP, Pietak AM, Huadmai J, Dias G. Magnesium and its alloys as orthopedic biomaterials: A review. Biomaterials. 2006; 27:1728–1734. [PubMed: 16246414]
2. Barfield WR, Colbath G, DesJardins JD, An YH, Hartsock LA. The potential of magnesium alloy use in orthopaedic surgery. Curr Orthop Pract. 2012; 23:146–150.
3. Zeng R, Dietzel W, Witte F, Hort N, Blawert C. Progress and challenge for magnesium alloys as biomaterials. Adv Eng Mater. 2008; 10:B3–B14.
4. Witte F, Hort N, Vogt C, Cohen S, Kainer kU, Willumeit R, Feyerabend F. Degradable biomaterials based on magnesium corrosion. Curr Opin Solid State Mater Sci. 2008; 12:63–72.
5. Witte F, Ulrich H, Palm C, Willbold E. Biodegradable magnesium scaffolds. II. Peri-implant bone remodeling. J Biomed Mater Res A. 2007; 81:757–765. [PubMed: 17390322]
6. Janning C, Willbold E, Vogt C, Nellesen J, Meyer-Lindenberg A, Windhagen H, Thorey F, Witte F. Magnesium hydroxide temporarily enhancing osteoblast activity and decreasing the osteoclast number in peri-implant bone remodelling. Acta Biomater. 2010; 6:1861–1868. [PubMed: 20035905]
7. Witte F, Ulrich H, Rudert M, Willbold E. Biodegradable magnesium scaffolds. I. Appropriate inflammatory response. J Biomed Mater Res A. 2007; 81:748–756. [PubMed: 17390368]
8. Castellani C, Lindtner RA, Hausbrandt P, Tschegg E, Stanzl-Tschegg SE, Zanoni G, Beck S, Weinberg AM. Bone-implant interface strength and osseointegration: Biodegradable magnesium alloy versus standard titanium control. Acta Biomater. 2011; 7:432–440. [PubMed: 20804867]
9. Witte F, Kaese V, Haferkamp H, Switzer E, Meyer-Lindenberg A, Wirth CJ, Windhagen H. In vivo corrosion of four magnesium alloys and the associated bone response. Biomaterials. 2005; 26:3557–3563. [PubMed: 15621246]
10. Lambotte A. L'utilisation du megnesium comme materiel perdu dans l'osteosynthese. Bull Mem Soc Nat Chir. 1932; 28:3557–3563.
11. Song G, Atrens A. Understanding magnesium corrosion: A framework for improved alloy performance. Adv Eng Mater. 2003; 5:837–858.
12. Kirkland NT, Lespagnol J, Birbilis N, Staiger MP. A survey of bio-corrosion rates of magnesium alloys. Corros Sci. 2010; 52:287–291.
13. Südholz AD, Birbilis N, Bettles CJ, Gibson MA. Corrosion behaviour of Mg-alloy AZ91E with atypical alloying additions. J Alloys Compd. 2009; 471:109–115.
14. Gu X, Zheng Y, Cheng Y, Zhong S, Xi T. In vitro corrosion and biocompatibility of binary magnesium alloys. Biomaterials. 2009; 30:484–498. [PubMed: 19000636]
15. Zainal Abidin NI, Martin D, Atrens A. Corrosion of high purity Mg, AZ91, ZE41 and Mg2Zn0.2Mn in Hank's solution at room temperature. Corros Sci. 2011; 53:862–872.
16. Salman SA, Ichino R, Okido M. A comparative electrochemical study of AZ31 and AZ91 magnesium alloy. Int J Corros. 2010; 2010:1–7.
17. Kannan BM, Singh RK. A mechanistic study of in vitro degradation of magnesium alloy using electrochemical techniques. J Biomed Mater Res A. 2010; 93:1050–1055. [PubMed: 19753621]
18. Hosny W, Ameer M. Electrochemical study and biological activity of AZ91E alloy in Hank's solution. Int J Electrochem Sci. 2013; 8:8371–8387.

19. Muller WD, Nascimento ML, Zeddies M, Corsico M, Gassa LM, Lorenzo de Mele MA. Magnesium and its alloys as degrabeable biomaterials. Corrosion studies using potentiodynamic and EIS electrochemical techniques. Mater Res. 2007; 10:5–10.
20. Gu XN, Zheng YF, Chen LJ. Influence of artificial biological fluid composition on the biocorrosion of potential orthopedic Mg-Ca, AZ31, AZ91 alloys. Biomed Mater. 2009; 4:065011. [PubMed: 19966381]
21. Xin Y, Liu C, Zhang X, Tang G, Tian X, Chu PK. Corrosion behavior of biomedical AZ91 magnesium alloy in simulated body fluids. J Mater Res. 2007; 22:2004–2011.
22. Witte F, Feyerabend F, Maier P, Fischer J, Stormer M, Blawert C, Dietzel W, Hort N. Biodegradable magnesium-hydroxyapatite metal matrix composites. Biomaterials. 2007; 28:2163–2174. [PubMed: 17276507]
23. Xue D, Yun Y, Tan Z, Dong Z, Schulz MJ. In vivo and in vitro degradation behavior of magnesium alloys as biomaterials. J Mater Sci Technol. 2012; 28:261–267.
24. Witte F, Reifenrath J, Müller PP, Crostack HA, Nellesen J, Bach FW, Bormann D, Rudert M. Cartilage repair on magnesium scaffolds used as a subchondral bone replacement. Materialwissenschaft und Werkstofftechnik. 2006; 37:504–508.
25. Yamamoto A, Hiromoto S. Effect of inorganic salts, amino acids and proteins on the degradation of pure magnesium in vitro. Mater Sci Eng C. 2009; 29:1559–1568.
26. Song G, Atrens A. Corrosion mechanisms of magnesium alloys. Adv Eng Mater. 1999; 1:11–33.
27. Kirkland, NT.; Birbilis, N. Magnesium Biomaterials: Design, Testing and Best Practice. Springer; New York: 2013. p. 132
28. Walker J, Shadanbaz S, Kirkland NT, Stace E, Woodfield T, Staiger MP, Dias GJ. Magnesium alloys: Predicting in vivo corrosion with in vitro immersion testing. J Biomed Mater Res B Appl Biomater. 2012; 100:1134–1141. [PubMed: 22331609]
29. Kirkland NT, Birbilis N, Staiger MP. Assessing the corrosion of biodegradable magnesium implants: A critical review of current methodologies and their limitations. Acta Biomater. 2012; 8:925–936. [PubMed: 22134164]
30. Seuss F, Seuss S, Turhan MC, Fabry B, Virtanen S. Corrosion of Mg alloy AZ91D in the presence of living cells. J Biomed Mater Res B Appl Biomater. 2011; 99:276–281. [PubMed: 21714090]
31. Bedjoudi T, Fiaud C, Robbiola L. Influence of homogenization and artificial aging heat treatments on corrosion behavior of Mg-Al alloys. Corros Sci. 1993; 49:738–745.
32. Lunder O, Lein JE, Aune T, Nisancioglu K. The role of Mg17Al12 phase in the corrosion of Mg alloy AZ91. Corrosion. 1989; 45:741–748.
33. Ehrensberger MT, Sivan S, Gilbert JL. Titanium is not “the most biocompatible metal” under cathodic potential: The relationship between voltage and MC3T3 preosteoblast behavior on electrically polarized cpTi surfaces. J Biomed Mater Res A. 2010; 93:1500–1509. [PubMed: 20014293]
34. Song G, Atrens A, Wu X, Zhang B-P. Corrosion behavior of AZ21, AZ501 and AZ91 in Sodium Chloride. Corros Sci. 1998; 40:1769–1791.
35. Singh Raman RK, Birbilis N, Efthimiadis J. Corrosion of Mg alloy AZ91—The role of microstructure. Corros Eng Sci Technol. 2004; 39:346–350.
36. Aung NN, Zhou W. Effect of heat treatment on corrosion and electrochemical behaviour of AZ91D magnesium alloy. J Appl Electrochem. 2002; 32:1397–1401.
37. Liu C, Xin Y, Tang G, Chu PK. Influence of heat treatment on degradation behavior of bio-degradable die-cast AZ63 magnesium alloy in simulated body fluid. Mater Sci Eng A. 2007; 456:350–357.
38. Zhou W, Shen T, Aung NN. Effect of heat treatment on corrosion behaviour of magnesium alloy AZ91D in simulated body fluid. Corros Sci. 2010; 52:1035–1041.
39. Wu G, Zhao Y, Zhang X, Ibrahim JM, Chu PK. Self-protection against corrosion of aged magnesium alloy in simulated physiological environment. Corros Sci. 2013; 68:279–285.
40. Zhao Y, Wu G, Jiang J, Wong HM, Yeung KWK, Chu PK. Improved corrosion resistance and cytocompatibility of magnesium alloy by two-stage cooling in thermal treatment. Corros Sci. 2012; 59:360–365.

41. Baril, Gv; Blanc, C.; Pébe?re, N. AC impedance spectroscopy in characterizing time-dependent corrosion of AZ91 and AM50 magnesium alloys characterization with respect to their microstructures. J Electrochem Soc. 2001; 148:B489.
42. Baril, Gv; Blanc, C.; Keddam, M.; Pébe?re, N. Local electrochemical impedance spectroscopy applied to the corrosion behavior of an AZ91 magnesium alloy. J Electrochem Soc. 2003; 150:B488.
43. Xin Y, Huo K, Hu T, Tang G, Chu PK. Corrosion products on biomedical magnesium alloy soaked in simulated body fluids. J Mater Res. 2009; 24:2711–2719.
44. Hiromoto S, Hanawa T. Electrochemical properties of 316L stainless steel with culturing L929 fibroblasts. J R Soc Interface. 2006; 3:495–505. [PubMed: 16849246]
45. Hiromoto S, Noda K, Hanawa T. Electrochemical properties of an interface between titanium and fibroblasts L929. Electrochim Acta. 2002; 48:387–396.
46. Garcia-Alonso MC, Saldana L, Alonso C, Barranco V, Munoz-Morris MA, Escudero ML. In situ cell culture monitoring on a Ti-6Al-4V surface by electrochemical techniques. Acta Biomater. 2009; 5:1374–1384. [PubMed: 19119085]
47. Gu X, Zheng Y, Zhong S, Xi T, Wang J, Wang W. Corrosion of, and cellular responses to Mg-Zn-Ca bulk metallic glasses. Biomaterials. 2010; 31:1093–1103. [PubMed: 19939446]
48. Mustafa K, Pan J, Wroblewski J, Leygraf C, Arvidson K. Electro-chemical impedance spectroscopy and X-ray photoelectron spectroscopy analysis of titanium surfaces cultured with osteoblast-like cells derived from human mandibular bone. J Biomed Mater Res. 2002; 59:655–664. [PubMed: 11774327]
49. Hiromoto S. Corrosion of metallic biomaterials in cell culture environments. Electrochem Soc Interface. 2008; 17:41–44.

FIGURE 1.

The three electrode corrosion cell used for concurrent cell culturing and electrochemical testing. The AZ91 working electrode is mounted at the bottom of the glass chamber. A graphite counter electrode and agar KCl salt bridge were suspended in the electrolyte. The KCl salt bridge provided an electrical connection to the reference well filled with PBS. [Color figure can be viewed in the online issue, which is available at wileyonlinelibrary.com.].

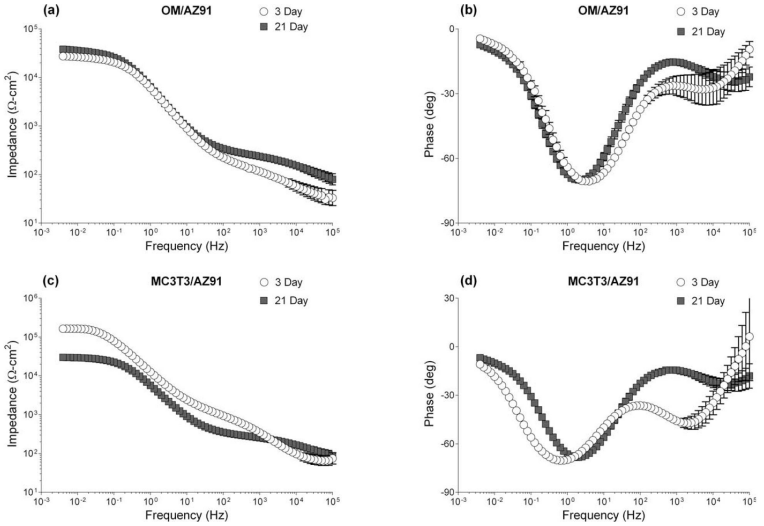

FIGURE 2.

Bode plots resulting from EIS of OM/AZ91 (a, b) and MC3T3/AZ91 (c, d) after 3 and 21 days of incubation in osteogenic media. Plotted data points represent the mean ± 1 standard deviation from three independent samples tested at each condition.

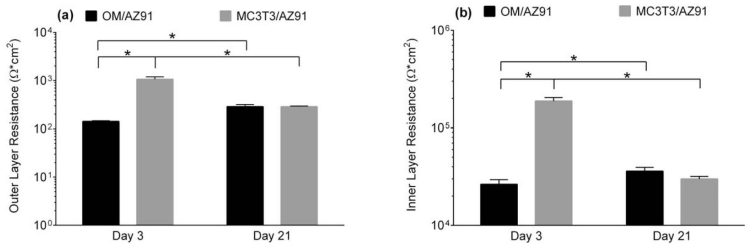

FIGURE 3.

Plots of the outer layer (a) and inner layer (b) resistance measured from EIS of OM/AZ91 and MC3T3/AZ91 after 3 and 21 days of incubation. The data are plotted as the mean ± 1 standard deviation of three independent samples for each group. *Indicates statistical difference ($p < 0.05$) between groups.

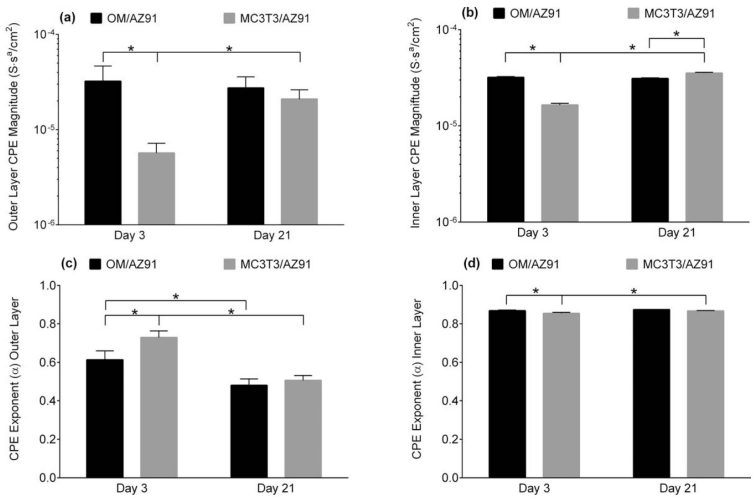

FIGURE 4.

Plots of the outer layer (a, c) and inner layer (b, d) of the CPE magnitude (a, b) and the CPE exponent (c, d) measured from EIS. The data are plotted as the mean ± 1 standard deviation of three independent samples for each group. *Indicates statistical difference ($p < 0.05$) between groups.

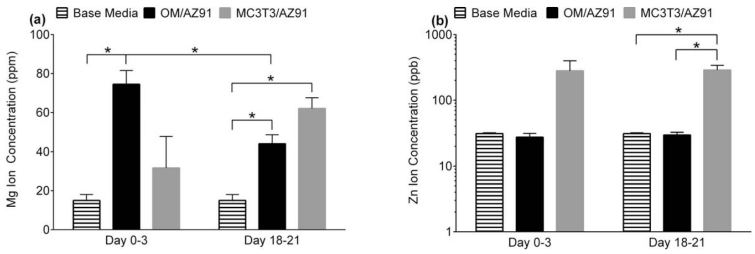

FIGURE 5.

Concentration of Mg (a) and Zn (b) ions present in the base media and released into the test solutions from 0 to 3 and 18 to 21 days of immersion of OM/AZ91 and MC3T3/AZ91 samples. The data are plotted as the mean ± 1 standard deviation of three independent samples for each group. *Indicates statistical difference ($p < 0.05$) between groups.

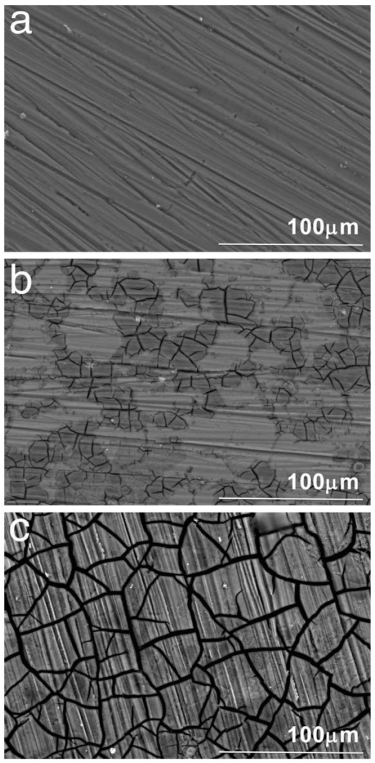

FIGURE 6.

Scanning electron micrographs of OM/AZ91 samples before immersion in osteogenic media (a), and after 3 days (b) and 21 days (c) of incubation. Distinct light and cracked regions were observed on 3-day samples.

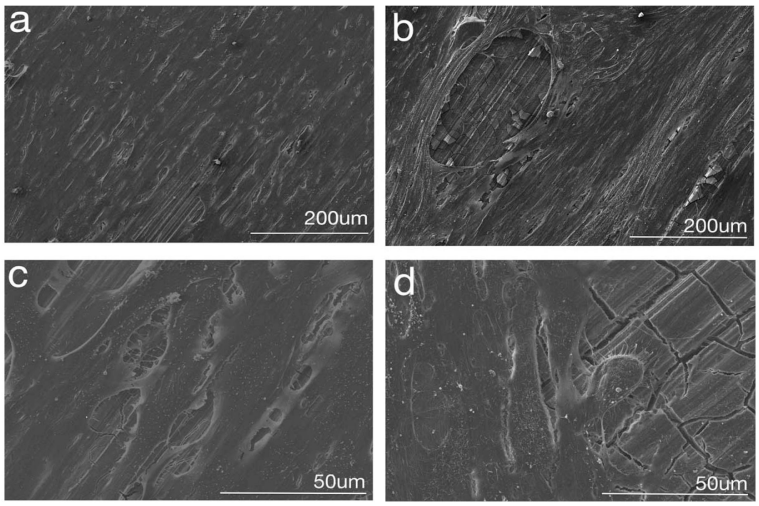

FIGURE 7.

Representative scanning electron micrographs of MC3T3/AZ91 samples after 3 (a, c) and 21 days (b, d) of cell culture.

TABLE I

Open circuit potential of OM/AZ91 and MC3T3/AZ91 samples after 3 and 21 days of incubation

	OM/AZ91 3 Day (a)	**OM/AZ91 21 Day (b)**	**MC3T3/AZ91 3 Day (c)**	**MC3T3/AZ91 21 Day (d)**	***p*-value (a vs. b)**	***p*-value (c vs. d)**	***p*-value (a vs. c)**	***p*-value (b vs. d)**
OCP (V vs. Ag/AgCl)	−1.55 ± 0.002	−1.51 ± 0.005	−1.56 ± 0.014	−1.54 ± 0.006	0.005	0.311	0.871	0.008

Results represent mean values ± 1 standard deviation for 3 independent samples. $p < 0.05$ was considered a statistical difference.

TABLE II

Results of Energy-Dispersive X-ray Spectroscopy for OM/AZ91 Samples After 0, 3, and 21 Days of Exposure to Osteogenic Media

	Atomic % ± SD				
	0 Days	3 Days			21 Days
Element	Total	Light	Cracked	Total	Total
O	1.5 ± 0.0	9.7 ± 0.4	61.7 ± 4.3	40.4 ± 3.3	70.6 ± 0.9
Mg	97.1 ± 0.1	83.6 ± 0.7	19.1 ± 7.3	46.8 ± 3.9	8.5 ± 1.6
Al	1.1 ± 0.0	5.8 ± 0.2	8.1 ± 0.5	6.9 ± 0.2	7.8 ± 0.1
P		0.8 ± 0.3	8.1 ± 1.7	4.4 ± 0.4	8.4 ± 0.4
Ca		0.2 ± 0.0	2.6 ± 1.0	1.3 ± 0.2	4.3 ± 0.4
Zn	0.1 ± 0.0	0.2 ± 0.0	0.4 ± 0.1	0.2 ± 0.0	0.2 ± 0.0

Atomic % values represent the mean % ± standard deviation (SD) for three independent samples at each time point.